GeoResJ 14 (2017) 36–46

Contents lists available at ScienceDirect

GeoResJ

journal homepage: www.elsevier.com/locate/georesj

The application of machine learning for evaluating anthropogenic versus natural climate change

John Abbot[a,b,c,*], Jennifer Marohasy[b,c]

[a] James Cook University, Townsville, Queensland, Australia
[b] Institute of Public Affairs, Melbourne, Victoria, Australia
[c] Climate Modelling Laboratory, Noosa, Queensland, Australia

ARTICLE INFO

Article history:
Received 22 April 2017
Revised 25 July 2017
Accepted 4 August 2017
Available online 5 August 2017

ABSTRACT

Time-series profiles derived from temperature proxies such as tree rings can provide information about past climate. Signal analysis was undertaken of six such datasets, and the resulting component sine waves used as input to an artificial neural network (ANN), a form of machine learning. By optimizing spectral features of the component sine waves, such as periodicity, amplitude and phase, the original temperature profiles were approximately simulated for the late Holocene period to 1830 CE. The ANN models were then used to generate projections of temperatures through the 20th century. The largest deviation between the ANN projections and measured temperatures for six geographically distinct regions was approximately 0.2 °C, and from this an Equilibrium Climate Sensitivity (ECS) of approximately 0.6 °C was estimated. This is considerably less than estimates from the General Circulation Models (GCMs) used by the Intergovernmental Panel on Climate Change (IPCC), and similar to estimates from spectroscopic methods.

1. Introduction

The past two decades have seen an unprecedented international focus on climate change, and particularly the perceived relationships between increasing global temperatures and emissions of greenhouse gases, referred to as anthropogenic climate change. The Intergovernmental Panel on Climate Change (IPCC) is a body under the auspices of the United Nations, set up at the request of member governments, to provide scientific information on climate change and its political and economic impacts. The IPCC publishes Assessment Reports at regular intervals, with the current viewpoint, based mainly on application of physical models, particularly General Circulation Models (GCMs). These models attribute over 90% of the global warming since 1900, and virtually 100% of the global warming since 1970, to anthropogenic climatic forcings, particularly industrial emissions of carbon dioxide and methane [71,87].

Instrumental temperature records extend back a little over a century. To understand how climate has varied over much longer periods, over hundreds and thousands of years, various types of proxy records have been assembled. These are derived from measurements associated with biological and geological phenomena that can leave evidence of past climate, particularly temperatures. The most familiar proxy records are derived from annual rings of long-lived tree species. Other proxies include measurements from corals, stalagmites, and sediments. These types of records provide evidence for periods of time over the past several thousand years (the late Holocene) that were either colder, or experienced similar temperatures, to the present, for example the Little Ice Age and the Medieval Warm Period [40,43,44].

Examination of many of these proxy temperature records shows they typically consist of complex oscillations or cycles about a mean value, with the amplitude and structure of the temperature signal depending on the geographical location considered. In the pre-industrial era, these oscillations represent the compound effect of natural phenomena both internal (e.g. North Atlantic Oscillation, El Nino Southern Oscillation) and external (e.g. solar, volcanic activity).

Since about the mid-nineteenth century, with the growth of industrialisation, there is the possibility that there is also a contribution to climate change from anthropogenic greenhouse gases, particularly carbon dioxide and methane. However, the relative contributions of natural cycles and anthropogenic effects is far from certain [94] and there is continuing interest in attempting to answer this question of relative contributions [10,35,64,67].

* Corresponding author at: Institute of Public Affairs, Melbourne, Victoria, Australia.
E-mail address: johnwabbot@gmail.com (J. Abbot).

http://dx.doi.org/10.1016/j.grj.2017.08.001
2214-2428/

There is an extensive literature examining the occurrence of periodic cycles within proxy temperature reconstructions, through application of spectral analysis [32,78,88]. Many of these studies also discuss possible relationships between these cyclic patterns in temperature profiles and natural phenomena that may affect causation, particularly those associated with solar cycles [14,27,40,56,74,81,82,97]. For example, in the southern hemisphere, Nordemann et al. [74] undertook spectral analysis using tree ring data from Brazil and Chile, providing evidence for associations with solar cycles, particularly the Suess (~200 year), Gleissberg (~90 years), Hale (~ 22 years) and Schwabe (11 years) cycles. Rigozoa et al. [79] examined tree ring widths in Chile, and found an association with solar activity with 11 and 80 year periodicities.

In the northern hemisphere, Raspopov et al. [78] performed spectral analysis of long-term dendrochronological data from Central Asia and demonstrated an approximate 200-year climatic periodicity, showing a high correlation with solar periodicity for the de Vries period (~210 years). Ogurtsov et al. [75] reported spectral analysis of tree periodicity and discussed the association with the modulation of regional climate in Northern Fennoscandia by the Gleissberg solar cycle (~90 years).

Moffa-Sánchez et al. [68] examined marine sediments for isotopic signals in the shells of the planktonic foraminifera over the past 1000 years. Spectral analysis showed a 200-year periodicity, identified with de Vries solar cycle (~210 years). Galloway et al. [32] generated a late Holocene temperature record based on diatoms from a sediment obtained from British Columbia, Canada. Spectral analysis shows significant periodicities at 42–60, 70–89, 241–243, and 380 years, and inferred relationships to sunspot number variation. Tan and Liu [89] produced a 2650-year temperature reconstruction from annual layers of a stalagmite from China, with spectral analysis indicating significant periodicities at 206 and 325 years.

Cyclic variations have also been associated with large-scale internal climate oscillatory modes [15], that may themselves in turn be influenced by solar activity [49,65,91,93,100,102]. For example, Wilson et al. [97] examined tree ring widths to enable a reconstruction over 1300 years for the Gulf of Alaska: identifying oscillatory modes at 90, 38, 24, 50.4 and 18.7 years related to changes in sea surface temperature pattern. In addition to the decadal and centennial cyclic periodicities referred to above, there is evidence of cycles on millennial time scales, for example the Bond and Dansgaard-Oeschger (DO) cycles [70,101].

These studies indicate that temperatures have oscillated at the regional and global scale with the resultant signals able to be decomposed into component parts. If a set of components can be identified, and given the very large datasets, at least in theory, the oscillations could be used to forecast future climate using machine learning techniques.

Artificial neural networks (ANNs) are a form of machine learning. The ANN technique has been widely applied to simulation and forecasting of climatic and meteorological variables including temperatures [18,26,76,80], rainfall [3,4,5,6,24,72,99] solar radiation [8,20], and wind speed [19,29,57]. In this study, proxy temperatures from the Canadian Rockies, Switzerland, Tasmania (Australia), New Zealand, southern South America and a composite representing the Northern Hemisphere, were decomposed into sets of sine waves. There are many such studies in the literature. However, what is unique with our study is that we have then used the resultant components to train ANNs and make projections of future temperature. The divergences between these projections based on the natural cycles, and actual temperature measurements from the twentieth century was used as an indication of the extent of anthropogenic influences contributing to global warming.

2. Methods

There are hundreds of proxy temperature records reported in the literature corresponding to the Holocene period – the last approximately 10,000 years. For this investigation, six proxy records were selected for further analysis, three from each hemisphere. For each hemisphere two proxy records selected corresponded to specific geographical locations, derived from one specific type of proxy. In addition, for each hemisphere, one multi-proxy record was selected corresponding to a wider geographical region.

Published graphical temperature proxy reconstructions were digitized using UN-SCAN-IT software. Table 1 gives a summary of the temperature proxy reconstructions used for analysis. The digitized time-series were then examined by spectral analysis using AutoSignal software, applying the Parametric Interpretation and Prediction tools with Fourier Transform analysis.

In each case, the number of sine curves applied to reconstruct the total signal was increased until the improvement in fitting, estimated by correlation coefficient, showed only marginal improvement. By adjustment of periodicities, phase and power of the identified sine wave components, the software optimizes simulations of the original proxy signal, using a defined number of component sine waves. In each case, the optimizations were undertaken from the proxy record start date through to 1830 CE. This can be regarded as a pre-industrial period, with only natural influences on climate (i.e. without anthropogenic/human-caused contributions).

Tables 2 and 3 show the results of spectral analysis for the three proxy records for the southern hemisphere and northern hemisphere respectively. The spectral analyses resulted in between 7 and 10 sine waves. The correlation was highest for the New Zealand tree ring data at 0.86, and lowest for the Tasmania tree ring data at 0.64.

In each case, this data based on the sinusoidal analysis, was used as the input data for subsequent machine learning. In particular, the data was provided as input to *Neurosolutions Infinity* software.

Many different architectures of ANNs have been used to make forecasts of climatic variables [1,3,24,72]. A common approach in the selection of an ANN architecture is through simple trial and error of candidate models [1–3]. With this very time-consuming approach, a limited set of input data is used and the machine learning topology and configuration chosen based on the error score. The selected model is then applied with all the data input sets.

In contrast, with *Neurosolutions Infinity* software, the configuration is automated. This offers a great advantage in terms of arriving at an optimum forecast model for every data set of interest without a prohibitive time outlay. The *Neurosolutions Infinity* program uses a pre-set formula incorporating Root Mean Square Error (RMSE), mean absolute error (MAE) and correlation coefficient (R) to evaluate the accuracy of different machine learning topologies and configurations for each set of selected inputs tested. Based on this formula, the program determines which model and set of inputs is optimal. Table 4 shows the range of machine learning topologies automatically tested using *Neurosolutions Infinity*, including different types of ANNs, fuzzy logic and support vector machines.

For the datasets used in this investigation, the optimal machine learning model automatically selected by *Neurosolutions Infinity* was a general regression neural network (GRNN) [85]. The topology of this type of ANN is shown in Fig. 5 as a feedforward network that can be used to estimate a vector Y from a measurement vector X. The network “learns” in one pass through the data and can generalize from examples as soon as they are stored. During training, the estimate converges to the conditional mean regression surfaces as more and more examples are observed. It forms very reasonable regression surfaces based on only a few samples,

Table 1
Summary of temperature proxy reconstructions used for analysis in this study.

Location	Proxy dates (AD)	Proxy types	Reference
Northern Hemisphere			
Swiss Alps	1200–1950	various lake sediments	[92]
Canadian Rockies	950–1975	tree rings	[56]
Northern hemisphere composite	50–2000	pollen, lake sediments, stalagmite, boreholes	[33]
Southern Hemisphere			
Southern south America multiproxy	900–1995	ice cores, tree rings, coral lake and marine sediment and instrumental data	[73]
South Island, New Zealand	900–2000	tree rings	[22]
Tasmania	1000–1980	tree rings	[22]

Table 2
Spectral analysis for proxy temperature series in the Southern Hemisphere to 1830.

Date range (AD)	New Zealand 900–1830		Southern South America 900–1830		Tasmania 1000–1830	
r^2	0.86		0.85		0.64	
Sine	Period (years)	Power (%)	Period (years)	Power (%)	Period (years)	Power (%)
1	715.9	2.6	745.4	28.9	648.0	13.4
2	283.1	1.5	383.3	23.6	277.8	15.1
3	154.8	24.5	245.4	14.2	167.2	7.9
4	148.5	56.8	216.6	3.1	78.9	14.1
5	140.0	10.6	140.9	15.3	63.0	11.9
6	107.5	0.8	129.2	6.5	56.0	24.1
7	83.8	1.0	89.2	6.0	46.1	13.5
8	67.0	0.6	52.0	2.3		
9	57.3	0.6				
10	51.1	1.0				

Table 3
Spectral analysis for proxy temperature series in the Northern Hemisphere to 1830.

Date range (AD)	Canada 950–1830		Switzerland 1200–1830		Northern hemisphere 50–1830	
r^2	0.70		0.80		0.72	
Sine	Period (years)	Power (%)	Period (years)	Power (%)	Period (years)	Power (%)
1	442.3	19.7	722.1	0.9	1227.6	2.7
2	270.7	29.6	345.8	2.1	428.1	34.2
3	190.1	27.6	138.1	0.2	422.3	39.3
4	119.1	10.5	104.9	0.7	148.5	11.5
5	68.7	6.7	78.7	1.1	147.7	11.7
6	46.5	3.2	67.7	0.2	128.9	0.1
7	41.9	2.9	35.5	46.4	106.1	0.2
8			35.4	48.2	82.4	0.1
9			25.5	0.3	76.4	0.1
10					55.0	0.1

Table 4
Machine learning topologies and configurations screened using *Neurosolutions Infinity*.

Machine learning topology	Configurations
Artificial neural network	Multilayer perceptron network
Artificial neural network	Jordan/Elmer networks
Artificial neural network	Time lag recurrent networks
Artificial neural network	Recurrent networks
Artificial neural network	Generalised regression neural networks (GRNN)
Fuzzy logic	CANFIS networks
Support vector machine	Support vector machine

Table 5
Fit for NZ tree ring proxy with training for the period 1000–1830AD.

	Spectral composite	ANN
RMSE	0.185	0.075
Correlation	0.870	0.979

and the estimate is bounded by the minimum and maximum of the observations. The GRNN is similar in form to the probabilistic neural network (PNN). Whereas the PNN finds decision boundaries between categories of patterns, GRNN estimates values for continuous dependent variables.

The GRNN has the following advantages: single-pass learning so no backpropagation is required; high accuracy in the estimation since it uses Gaussian functions; and, it can handle noises in the inputs (Fig. 1).

A composite signal can be constructed from the sets of component sine waves through simple addition of the sinusoidal components. This composite signal can itself be used as the basis of making projections of temperature. However, superior fitting to the temperature proxies are obtained by using the sine wave components and composite as input data. This was established by comparing the spectral analysis composite method versus the ANN method for the training periods. The ANN method gave a higher correlation and lower RMSE and therefore was judged superior, as illustrated by the comparative results for the New Zealand data in Table 5.

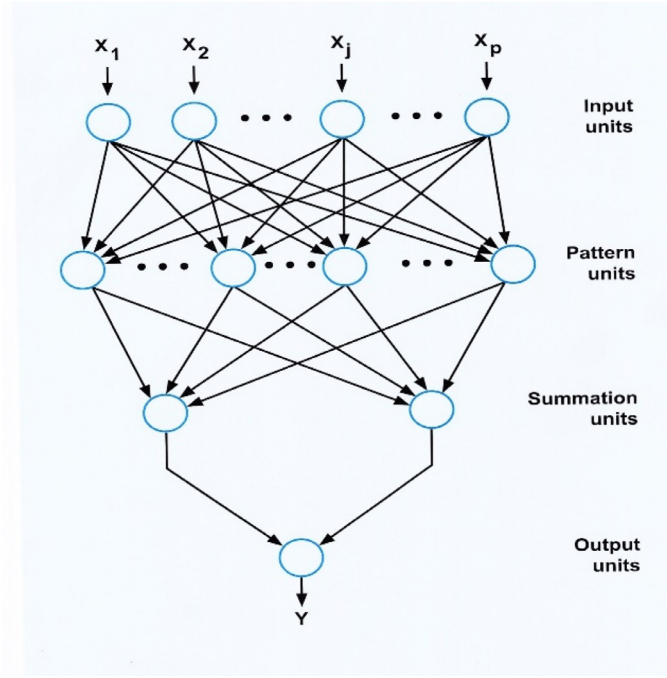

Fig. 1. Topology of the generalised regression neural network (GRNN).

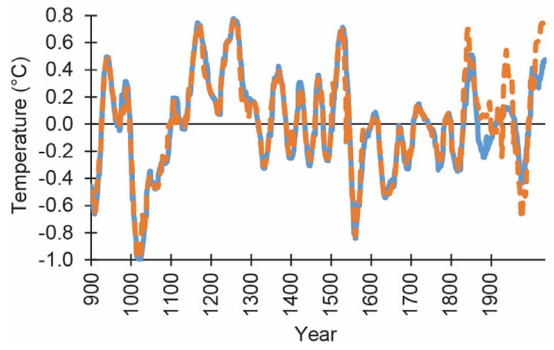

Fig. 2. Proxy temperature record (blue) and neural network output (orange) based on input from spectral analysis for New Zealand tree rings proxy. Training period 900–1830; test period 1830–2000. (For interpretation of the references to colour in this figure legend, the reader is referred to the web version of this article.)

3. Results

ANN models were generated for each of the six proxy records shown in Table 1, with the proxy data and also the corresponding values from the spectral analysis used as input. Output from each of these models has been charted for the entire proxy period – enabling visual assessment of trends and also deviations between the proxy temperature record and the ANN model outputs, as shown in Figs. 2, 4, 6, 8, 10, and 12. In each chart, the blue line represents the observed/measured proxy values, and the orange line is the ANN output. The ANN output corresponds to an optimization of parameters with a training period from the start of the proxy record to 1830. For the periods from 1830 to the end of each proxy record, the ANN output corresponds to a projection using the parameters generated in the training process.

Of particular interest is the test period corresponding to the post-industrial era from 1880 to 2000 associated with introduction of anthropogenic greenhouse gases into the atmosphere, and so this period is shown in more detail for each record in Figs. 3, 5, 7, 9, 11 and 13.

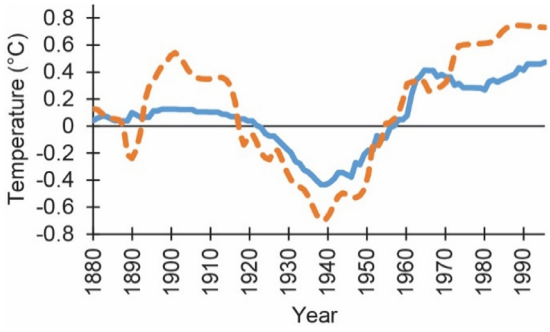

Fig. 3. Proxy temperature record (blue) and neural network projection (orange) for New Zealand tree rings proxy for test period between 1880–2000. (For interpretation of the references to colour in this figure legend, the reader is referred to the web version of this article.)

Table 6
Selected inputs for New Zealand tree ring proxy temperatures.

Inputs	Contribution (%)
Sum (Sine 6, Composite)	26.4
Sine 4	25.9
Sum (Sine 7, Composite)	25.5
Sum (Sine 10, Composite)	22.3

Table 7
Selected inputs for southern South America proxy temperatures.

Inputs	Contribution (%)
Sum(Sine 1, Composite)	45.8
Minimum(Sine 1, Composite)	38.8
Sine 8	15.4

Table 8
Selected inputs for Tasmanian tree ring proxy temperatures.

Inputs	Contribution (%)
Sine 4	18.7
Sine 5	18.4
Sine 7	16.5
Sine 2	11.6
Sine 1	11.5
Sum (Sine1, Sine2)	8.4
Sum (Sine 1, Sine 2, Sine 4, Sine 5)	14.8

Tables 6–11 show the corresponding sets of spectral inputs selected by *Infinity* for the optimised ANN models. In the case of New Zealand, for example, four inputs were used to build the ANN model, each contributing between 22% and 26% to the model, as shown in Table 6.

The proxy measurements suggest New Zealand's climate has fluctuated within a band of approximately 2 °C since at least 900 CE, as shown in Fig. 2. The warming of nearly 1 °C since 1940 falls within this band. The discrepancy between the orange and blue lines in recent decades as shown in Fig. 3, suggests that the anthropogenic contribution to this warming could be in the order of approximately 0.2 °C.

Seven different sine waves were used by the ANN in the building of the model using the South American data, as shown in Table 7. The proxy measurements indicate temperatures have historically fluctuated within a band of approximately 1 °C. The measurements since 1880 show a gradual increase, with the proxy measurements to 2000 slightly higher than the projection by the ANN model.

Table 9
Inputs for Canadian Rockies tree rings proxy temperatures.

Inputs	Contribution (%)
Sine 3	26.2
Sine 2	15.5
Sine 1	13.8
Sine 7	4.2
Composite	27.5
Sum(Composite, Sine2)	12.8

Table 10
Inputs for Swiss varved lake sediment proxy temperatures.

Inputs	Contribution (%)
Sine 8	21.8
Sine 6	20.2
Composite	19.4
Difference (Sine 9, Sine 2)	17.2
Sine 2	13.0
Minimum(Sine 6, Sine 2)	8.5

Table 11
Inputs for northern hemisphere multi-proxy temperatures.

Inputs	Contribution (%)
Minimum(Composite, Sine 1, Sine 7)	36.7
Sum(Composite, Sine 1, Sine 3, Sine 7)	28.2
Minimum(Sine 1, Sine 9)	18.8
Minimum(Sine 9, Sine 1)	16.3

The Tasmanian tree ring proxies also fluctuate within a band of approximately 1 °C, but showing a significant fall in temperatures in the early 1900s, evident in Figs. 6 and 7. The ANN projects an increase that is somewhat less than measurements from the proxies, as shown in Fig. 7.

The proxy record from the Canadian Rockies oscillates within a slightly broader band and shows a more consistent warming trend since the 1880, as evident in Figs. 7 and 8.

The proxy measurements from Switzerland suggest more recent oscillations, with temperatures hotter in the late 1800s, cooling, and then increasing towards the middle of last century – as shown in Figs. 10 and 11. The record for the entire Northern Hemisphere suggests warming to 1000 CE, then cooling through a period known as The Little Ice Age, before the recent warming, Figs. 12 and 13.

To summarize, Figs. 3, 5, 7, 9, 11 and 13 indicate that the period from 1880 to the end of the proxy records shows general correspondence between the projections generated by ANN output (which is based on input using extrapolation of natural oscillations from the pre-industrial era), and the actual proxy temperature measurements. Importantly, an upward trend is generally apparent for both the proxy measurements and the ANN model projection for the 20th century. This would suggest that the increase in temperature over the last 100 years can be largely attributed to natural phenomena.

The actual measured deviations between the proxy temperature record and neural network projection from 1880 are shown in Table 12. Values are based on the mean absolute errors between proxy measurements and model projection.

Table 12
Average deviation between proxy temperature record and ANN projection for the period from 1880 to end of proxy records.

Location	Deviation (°C)
Canadian Rockies	0.06
Northern Hemisphere	0.09
Switzerland	0.20
Tasmania	0.14
New Zealand	0.20
Southern South America	0.06

4. Discussion

The most recent IPCC report AR5 [87] states that global averaged surface temperatures increased by 0.85 °C for the period 1880 to 2012, and that most of the warming since 1900 is attributable to increasing atmospheric concentrations of greenhouse gases from human emissions. This finding is based on calculations derived from the output of GCMs, with the mean equilibrium climate sensitivity (ECS) based on 30 of these models determined to be 3.2 °C [30], as shown in Table 13.

The ECS refers to the equilibrium change in global mean near-surface air temperature that would result from a sustained doubling of the atmospheric (equivalent) carbon dioxide concentration. It is derived from the GCMs, together with a set of external radiative forcing (RF) functions [11,30,71]. The external radiative forcing functions were initially based on the work of Svante Arrhenius in the 19th century, who first proposed that a doubling of atmospheric carbon dioxide could lead to a 5 to 6 °C increase in global temperatures [12]. These estimates have since been progressively revised down, but are generally much larger than estimates from those working from a basis of experimental spectroscopy, as shown in Table 13.

A key difference in the results from spectroscopy versus GCMs relates to the treatment of water vapour. IPCC-affiliated climate scientists explicitly excluded water vapour in the calculation of radiative forcing. While early experimental work quantified the molecular absorption, radiation and collisional interactions of carbon dioxide relative to the other dominant greenhouse gases including water vapour because of the partial overlap in absorption bands and therefore competition between these gases for available infrared radiation [13].

Lightfoot and Mamer [50], like Barrett [13], consider water vapour the dominant greenhouse gas, and use spectroscopic analysis and worldwide hourly measurements of atmospheric temperature and relative humidity to estimate an ECS of only 0.33 °C for a doubling of carbon dioxide, as shown in Table 13. Laubereau and Iglev [45] reported measurements in the infrared region with pure CO_2 using a cell of path length 10 cm. These laboratory spectroscopy results were then applied to a five-layer atmospheric model, including a surface layer and four layers to quantify greenhouse effect. Using the reported increase in atmospheric CO_2 concentration from 290 to 385 ppm between 1880 and 2010. These researchers derived a direct temperature rise attributable to CO_2 of about 0.26 °C. Even including the simultaneous feedback effect of atmospheric water vapour, they determined that CO_2 contributed somewhat less than 33% of its reported contribution to reported global warming of approximately 1.2 °C. Based on spectroscopic studies, Wilson and Gea-Banacloche [98] also suggest an ECS of less than 1 °C, as shown in Table 13.

There is an order of magnitude difference between the ECS estimates in the latest IPCC report [87] and the findings from these spectroscopic methods.

Our technique using spectral analysis and machine learning represents an alternative way of calculating an approximate ECS value, and thus potentially reconciling the difference between the output from GCMS and the results from spectroscopy – and indeed the other methods listed in Table 13. In particular, by calculating the difference between the temperatures actually recorded in the 20th century, and values that are likely to have been recorded in the ab-

Table 13
Methods for separating natural and anthropogenic climatic temperature variation and associated values of equilibrium climate sensitivity (ECS).

Reference	Equilibrium Climate Sensitivity (°C)	Range (°C)	Method
1. General Circulation Models/Radiative Forcing			
[30] (Table 9.5)	3.2	2–4.5	
2. Energy balance models			
[84]	1.8	0.9–3.2	Ocean heat content and global temperatures
[46]	1.64	1.25–2.45	Global energy budget
[38]	0.6	0.5–0.7	Two layers (atmosphere and ground) acting simultaneously as absorbers and Planck radiators, with additional heat transfer between these layers due to convection and evaporation.
[47]	1.66	0.7–3.2	Energy balance model using ocean diffusivity
[52]	0.6		Fluctuations in sea surface temperatures and concurrent fluctuations in top-of-atmosphere outgoing radiation
[9]	2.0	1.2–3.5	Ocean heat content and global temperature
[16]	1.9	1.2–2.6	Ocean heat content and global temperature
[61]	1.98	1.19–5.15	Ocean heat content and surface temperatures
[86]	0.4		Heat transfer/radiation exchange
3. Oscillatory cycles			
[95]	2.0	1.7–2.3	Multi-scale climate response model fitted to temperature records with time scales ranging from a year to a millennium, linked to solar irradiance
[55]	1.99	1.75–2.23	Periodic temperature oscillations associated with the Pacific Decadal Oscillation and Atlantic Multidecadal Oscillation
[82]	1.5	1.0–2.3	Model based on decadal and multi-decadal oscillations with astronomical origins
Present study	0.6–0.8		
4. Spectroscopic methods			
[50]	0.33		Experimental measurements
[45]	0.8		Spectroscopic measurements on optically thick samples of CO_2
[98]	0.9		Spectroscopy and radiative transfer equations
5. Palaeoclimate studies			
[83]	2.3	1.7–2.6	Sea and land surface temperature reconstructions from last glacial maximum
[39]	2.5		Model using last glacial maximum

sence of human emission of carbon dioxide, using a projection of the neural network output based on optimisations in neural network training periods prior to 1830.

The values in Table 12 show the average deviation between the measured proxy temperatures and the ANN projections for the period from 1880 – assuming a set of natural oscillatory cycles unaffected by human emissions. The average deviation varies from 0.06 to 0.20 °C. Taking the largest value of 0.20 °C, which represents the greatest potential difference between anticipated and actual temperatures during a period when carbon dioxide levels increased by approximately 100 ppm, we calculate an estimated ECS of 0.6 °C for a doubling of atmospheric carbon dioxide. This is a crude estimate, and it is of the same order of magnitude as the estimates using spectroscopic methods, as shown in Table 13.

Our method for calculating an ECS is possible because the ANN models could effectively reproduce historical temperature profiles, as shown by Figs. 2, 4, 6, 8, 10 and 12. The historical profiles indicate that prior to industrialization the climate underwent oscillations up to approximately 1 °C either side of a mean value, and that this pattern continued into the 20th century. The proxy measurements based on tree rings from New Zealand, for example, indicate that temperatures fluctuated naturally within a band of approximately 2 °C. The proxy measurements from 1880 to 1940 shows overall cooling for this region. This is inconsistent with global trends, but consistent with the raw instrumental record for nearby eastern and south-eastern Australia [25,60].

As pointed out by Scafetta [82], a major limitation of GCMs is that they do not adequately generate the necessary amplitude of temperature oscillations apparent in proxy records extending back over several millennia. The relatively small attribution to natural phenomena leads to temperature profiles typified by the “hockey stick” [58,59]. However, the majority of proxy temperature profiles found in the literature over the past several millennia, whether local or regional, do not resemble this hockey stick profile, but rather exhibit significant amplitude in oscillations over the past several millennia. For example, many regional temperature proxies for the northern hemisphere show pronounced cyclical behaviour corresponding to the Medieval Warm Period (MWP) and the Little Ice Age (LIA) [36,54,77,90], as shown in Fig. 12.

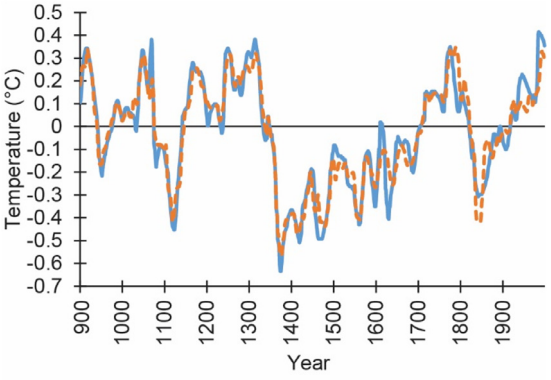

Fig. 4. Proxy temperature record (blue) and neural network output (orange) based on input from spectral analysis for regional southern South America multiproxy temperatures. Training period 900–1830; test period 1830–1995. (For interpretation of the references to colour in this figure legend, the reader is referred to the web version of this article.)

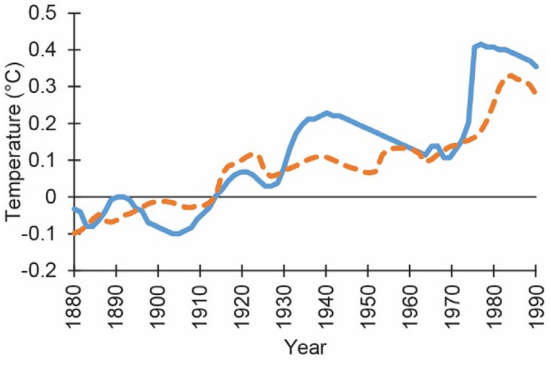

Fig. 5. Proxy temperature record (blue) and neural network projection (orange) for regional southern South America for test period 1880–1995. (For interpretation of the references to colour in this figure legend, the reader is referred to the web version of this article.)

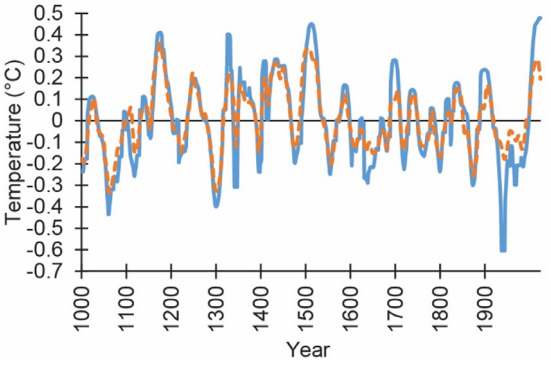

Fig. 6. Proxy temperature record (blue) and neural network projection (orange) based on input from spectral analysis for Tasmanian tree ring proxy temperatures. Training period 1000–1830; test period 1830–1980. (For interpretation of the references to colour in this figure legend, the reader is referred to the web version of this article.)

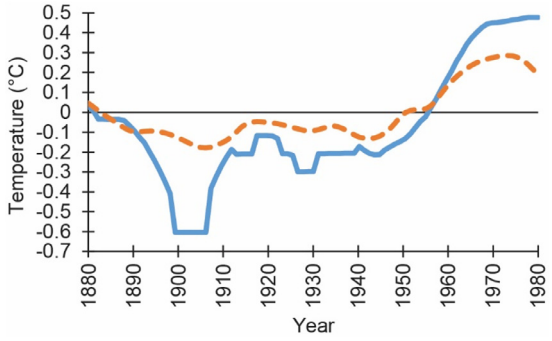

Fig. 7. Proxy temperature record (blue) and neural network projection (orange) for Tasmanian tree ring proxy temperatures for test period 1880–1980. (For interpretation of the references to colour in this figure legend, the reader is referred to the web version of this article.)

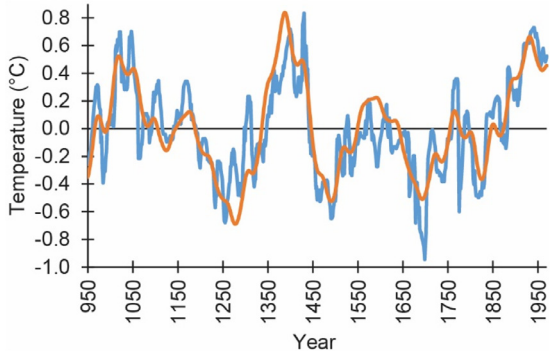

Fig. 8. Proxy temperature record (blue) and neural network projection (orange) based on input from spectral analysis for Canadian Rockies tree-ring proxy temperatures. Training period 950–1830; test period 1830–1975. (For interpretation of the references to colour in this figure legend, the reader is referred to the web version of this article.)

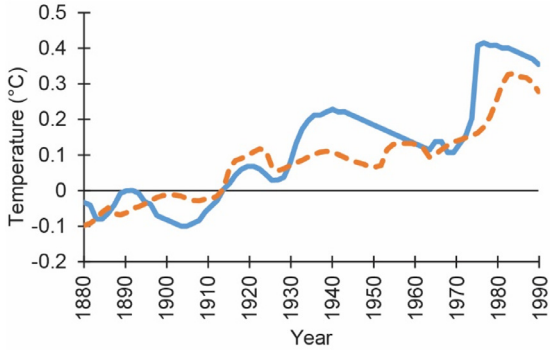

Fig. 9. Proxy temperature record (blue) and neural network projection (orange) based on input from spectral analysis for Canadian Rockies tree-ring proxy temperatures for test period 1880–1975. (For interpretation of the references to colour in this figure legend, the reader is referred to the web version of this article.)

As illustrated in the IPCC AR5, the output of some GCMs can reasonably replicate the observed global mean surface temperature profile between 1860 and 2010 with appropriate selection of natural and anthropogenic forcings (Fig. 10.1, [17]). However as discussed by Scafetta [81] in contrasting hockey stick temperature reconstructions [23,58] against many temperature reconstructions of the Norther Hemisphere [21,53,59,66], there are shortcomings when the past several millennia are considered. As pointed out by Scafetta [81], while the temperature reconstruction from GCMs predict a cooling of just about 0.2 °C, or less, from the Medieval Warm Period to the Little Ice Age of the 16–19th centuries, many Northern Hemisphere temperature reconstructions actually show a variability during the same period of about 0.6–0.7 °C. The large climatic variability observed since the medieval times can be correctly interpreted only if the climatic effects of natural variations, such as solar variability, on the climate have been severely underestimated by the climate models by a 3 to 6 factor and simultaneously the climatic effect of the radiative forcings, including the CO_2 forcing, has been overestimated by at least a factor of 2 [48].

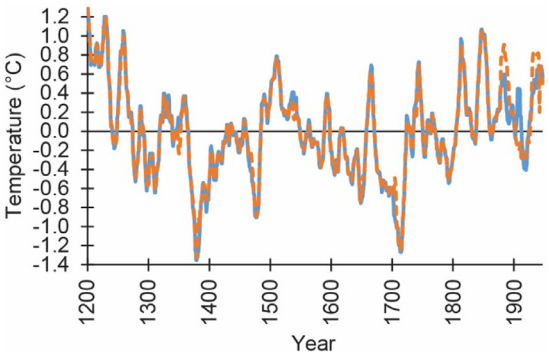

Fig. 10. Proxy temperature record (blue) and neural network projection (orange) based on input from spectral analysis for Swiss varved lake sediment proxy temperatures. Training period 1200 – 1830; test period 1830–1950. (For interpretation of the references to colour in this figure legend, the reader is referred to the web version of this article.)

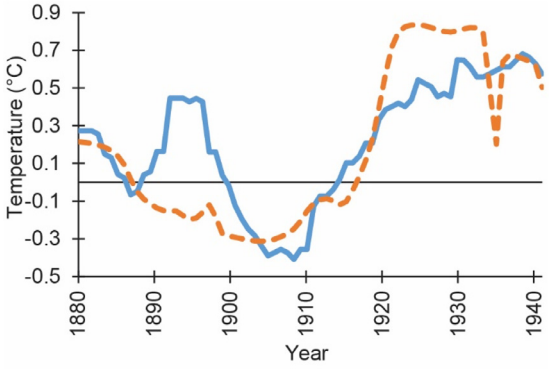

Fig. 11. Proxy temperature record (blue) and neural network projection (orange) for Swiss varved lake sediment for test period 1880–1950. (For interpretation of the references to colour in this figure legend, the reader is referred to the web version of this article.)

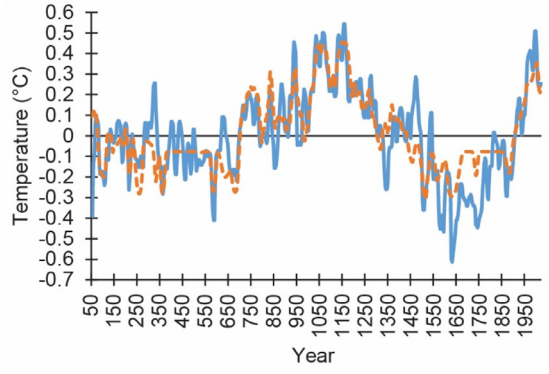

Fig. 12. Proxy temperature record (blue) and neural network projection (orange) based on input from spectral analysis for northern Hemisphere multiproxy. Training period 50 to 1830; test period 1830–2000. (For interpretation of the references to colour in this figure legend, the reader is referred to the web version of this article.)

The occurrence of a period as warm as the present, back approximately 1000 years, is also supported by oral histories [44] and detailed archaeological research [69]. For example, excavation of Inuit and Norse settlements in Northwest Greenland indicate this region was only inhabitable for a period from 985 CE until approximately 1200 CE [42,62,63]. The subsequent period corresponding to the Little Ice Age in the proxy temperature record was too cold for human inhabitation of Greenland. Colonisation in recent times again corresponds with the recent warmer epoch – with continuous colonisation of Upernavik not possible until 1826 [96]. The

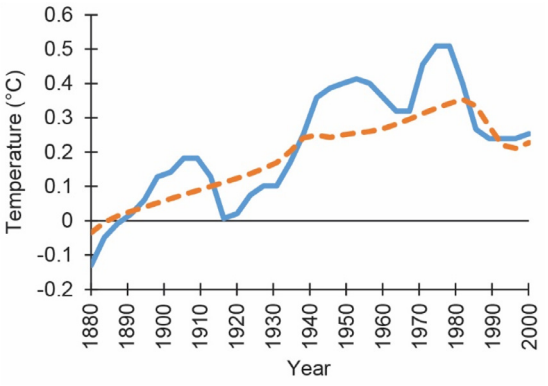

Fig. 13. Proxy temperature record (blue) and neural network projection (orange) based on input from spectral analysis for northern Hemisphere multiproxy for test period 1880–2000. (For interpretation of the references to colour in this figure legend, the reader is referred to the web version of this article.)

changes in the local climatic conditions are thought to have been a consequence of change in global oceanic circulation patterns, which manifested as changes in the strength of the sea current in the Davis Strait, which in turn affected the quantity, frequency and time of arrival of sea ice [96].

Our research was also informed by other studies based on natural oscillations, as listed in Table 13. As in the present study, Loehle [55] and Scafetta [82] take the approach that sets of natural cycles are embedded in both proxy and instrumental temperature profiles. If these cycles can be at least approximately quantified, then the residual temperature changes not accounted for in simulations of the combination of oscillations can be associated with anthropogenic radiative forcings during the industrial era.

One approach is to initially specify a set of well-defined oscillations associated with natural phenomena. For example, Loehle [55] considered two internal periodic temperature oscillations, associated with the Pacific Decadal Oscillation and the Atlantic Multidecadal Oscillation. The combined effect of these two oscillations was subtracted from surface temperature data to leave a linear signal, identified with an anthropogenic influence corresponding to an ECS of 1.99 °C. Zhou et al. [104] reported that when natural oscillations are considered, in particular the Atlantic multi-decadal oscillation, previous estimations of anthropogenic warming need to be substantially reduced, probably by a factor of at least 2.

Another approach is to examine temperature profiles using spectral analysis to identify a set of oscillations, which may subsequently, at least tentatively, be associated with known natural cycles. Scafetta [82] concluded that 50–60% of the recent post-industrial global warming can be attributed to natural oscillations particularly of solar origin, corresponding to an ECS value of 1.5 °C. He pointed out that the oscillations are not reproduced by current GCMs, and consequently these models omit important 'forcings' of the climate system and related feedbacks. This model comprised six oscillatory modes corresponding to a set of six oscillations with periods of about 9.1, 10–12, 19–22 and 59–63, ~115 and (~983 years) plus a climate component regulated by the chemical properties of the atmosphere (e.g. greenhouse gases and aerosols).

The approach used in the present investigation first applies spectral analysis to generate a set of sine waves, and subsequently, in the second step uses this data as input into a neural network. This potentially enables greater flexibility in fitting the temperature profiles during the training process. As one moves from the simplest approach, specifying the oscillations, then to application of spectral analysis, and finally to the application of both spectral analysis neural networks, the value of the associated ECS decreases (Table 13) as might be expected with fewer constraints imposed.

A fourth method of calculating ECS relies on application of energy balance models to the atmosphere and oceans to account for transfer of heat and temperature variations. Examples of these investigations are shown in Table 13, with ECS values in the range 0.6 to 2.0 °C. These values are also lower than the mean value of 3.2 °C derived from GCMs, again suggesting that there would be a requirement for increased contributions associated with natural phenomena to explain the observed 20th century warming. Furthermore, the lowest estimates from these models correspond with our estimate of 0.6 °C.

The final method illustrated in Table 13 is associated with palaeo-climatic studies [28]. For example, Lim et al. [51] concluded, from proxy-based investigations, that both cyclical solar forcing as well as the anthropogenic greenhouse gas forcing have been important in increasing the global mean temperature during the present warm period. Using climate proxy data, they suggested that solar forcing explains 30–50%, and greenhouse gas forcing explain 50–70% of the increase in global mean surface temperatures during this period, respectively. Table 13 shows examples of investigations using palaeo-climatic studies generating ECS values of 2.3 and 2.5 °C.

While global trends can be calculated, there is significant geographic variability and this further adds to the large uncertainties in the relative contributions of anthropogenic and natural phenomena to global warming in the industrial era [7,31,34,73,103].

There is obvious merit in attempting to construct physical models to understand simulate and forecast climatic phenomena. However the inherent complexity of the earth's climatic system should lead to caution in the confidence of model outputs, particularly when important characteristics such as oscillatory behaviour [81] and the late 20th century hiatus in atmospheric temperature increase [37,41] are not well replicated in outputs. An alternative is to approach, as demonstrated here, does not require a prior understanding of the physical processes, but adequate data and appropriate machine learning techniques. This approach may also eventually lead to better understanding of the physical processes through identification of important cyclical phenomena and their interactions. In some cases it has been demonstrated that the machine learning approach consistently outperforms the physical models, for example when applied to medium-term rainfall forecasting [5,6].

5. Conclusions

The uptake of machine learning, and specifically ANNs, in climate science has generally been slow compared to many other fields. This may in part be due to the heavy investment in physical models, particularly GCMs, over the past two decades and their importance to the theory of anthropogenic global warming. However, the complexity of the climate systems and limited understanding of all the physical processes leads to large uncertainties in the results generated –including the Equilibrium Climate Sensitivity (ECS). The present investigation attempts to reconcile ECS calculations from GCMs versus experimental methods.

Using proxy records from a limited number of geographic locations, decomposing these through signal analysis and then using the resulting component sine waves as input into ANN models has enabled us to generate projections of temperatures for the period from 1880 to 2000 based on natural climate cycles. These temperature projections indicate warming due to natural climate cycles would be in the range 0.6 to 1 °C, depending on geographical location. The difference between our model output and actual recorded values was at most 0.2 °C. Knowing the corresponding rise in atmospheric carbon dioxide levels over this same period has enabled us to estimate an ECS of 0.6 °C, which is approximately equivalent to values from experimental spectroscopic studies and the lowest estimates from energy balance models.

Acknowledgement

This research was funded by the B. Macfie Family Foundation.

References

[1] Abbot J, Marohasy J. Application of artificial neural networks to rainfall forecasting in Queensland, Australia. Adv Atmos Sci 2012;29(4):717–30.
[2] Abbot J, Marohasy J. The potential benefits of using artificial intelligence for monthly rainfall forecasting for the Bowen Basin, Queensland, Australia. WIT Trans Ecol Environ 2013;171:287–97.
[3] Abbot J, Marohasy J. Input selection and optimisation for monthly rainfall forecasting in Queensland, Australia, using artificial neural networks. Atmos Res 2014;138:166–78.
[4] Abbot J, Marohasy J. Forecasting monthly rainfall in the Bowen Basin of Queensland, Australia, using neural networks with Niño Indices. Lect Notes Artif Int 2016;9992:88–100.
[5] Abbot J, Marohasy J. Skilful rainfall forecasts from artificial neural networks with long duration series and single-month optimization. Atmos Res 2017;197:289–99.
[6] Abbot J, Marohasy J. Application of artificial neural networks to forecasting monthly rainfall one year in advance for locations within the Murray Darling Basin, Australia. Int J Sus Dev Plann 2017;12(8):1282–98.
[7] Abram NJ, McGregor HV, Tierney JE, Evans MN, McKay NP, Kaufman DS, et al. Early onset of industrial-era warming across the oceans and continents. Nature 2016;536(7617):411.
[8] Al-Shamisi MH, Assi AH, Hejase HAN. Artificial neural networks for predicting global solar radiation in Al Ain City – UAE. Int J Green Energy 2013;10(5):443–56.
[9] Aldrin M, Holden M, Guttorp P, Skeie RB, Myhre G, Berntsen TK. Bayesian estimation of climate sensitivity based on a simple climate model fitted to observations of hemispheric temperatures and global ocean heat content. Environmetrics 2012;23:253–71.
[10] Andres HJ, Peltier WR. Attributing observed Greenland responses to natural and anthropogenic climate forcings. Clim Dyn 2015;45:2919–36.
[11] Andrews T, Gregory JM, Webb MJ, Taylor KE. Forcing, feedbacks and climate sensitivity in CMIP5 coupled atmosphere-ocean climate models. Geophys Res Lett 2012;39:L09712.
[12] Arrhenius S. On the influence of carbonic acid in the air upon the temperature of the ground. Philos Mag 1896;41(5):237–76.
[13] Barrett J. Greenhouse molecules, their spectra and function in the atmosphere. Energy Environ 2005;16(6):1037–45.
[14] Beer J, Mende W, Stellmacher R. The role of the sun in climate forcing. Quat Sci Rev 2000;19:403–15.
[15] Bengtsson L. What is the climate system able to do 'on its own'? Tellus B 2013;65:20189.
[16] Bengtsson L. Schwartz SE Determination of a lower bound on Earth's climate sensitivity. Tellus B 2013;65:21533.
[17] Bindoff NL, Stott PA, AchutaRao KM, Allen MR, Gillett N, Gutzler D, et al. Detection and attribution of climate change: from global to regional Climate change 2013: the physical science basis. Contribution of working group I to the fifth assessment report of the intergovernmental panel on climate change Cambridge University Press Cambridge, United Kingdom and New York, NY, USA; 2013.
[18] Cakir S, Kadioglu M, Cubukcu N. Multischeme ensemble forecasting of surface temperature using neural network over Turkey. Theor Appl Climatol 2013;111(3-4):703–11.
[19] Cardenas-Barrera JL, Meng J, Castillo-Guerra E, Chang L. A neural network approach to multi-step-ahead, short-term wind speed forecasting. In: 12th International conference on machine learning and applications (ICMLA), 2; 2013. p. 243–8.
[20] Chen SX, Gooi HB, Wang MQ. Solar radiation forecast based on fuzzy logic and neural networks. Renew Energy 2013;60:95–201.
[21] Christiansen B, Ljungqvist FC. The extra-tropical Northern Hemisphere temperature in the last two millennia: reconstructions of low-frequency variability. Clim Past 2012;8:765–86.
[22] Cook ER, Buckley BM, Palmer JG, Fenwick P, Peterson MJ, Boswijk G, et al. Millennia-long tree-ring records from Tasmania and New Zealand: a basis for modelling climate variability and forcing, past, present and future. J Quat Sci 2006;21(7):689–99.
[23] Crowley TJ. Causes of climate change over the past 1000 years. Science 2000;289:270–7.
[24] Darji MP, Dabhi V, Harshadkumar BP. Rainfall forecasting using neural network: a survey. International conference on advances in computer engineering and applications (ICACEA); 2015.
[25] Deacon EL. Climatic change in Australia since 1880. Austr J Phys 1952;6:209–18.
[26] De SS, Chattopadhyay G, Bandyopadhyay B, Suman P. A neurocomputing approach to the forecasting of monthly maximum temperature over Kolkata, India using total ozone concentration as predictor. C R Geosci 2011;343(10):664–76.

[27] Dergachev VA, Raspopov OM. Reconstruction of the Earth's surface temperature based on data of deep boreholes, global warming in the last millennium, and long-term solar cyclicity. Part 2. Experimental data analysis. Geomagn Aeronomy 2010;50(3):393–402.
[28] Edwards TL, Crucifix M, Harrison SP. Using the past to constrain the future: how the palaeorecord can improve estimates of global warming. Prog Phys Geog 2007;31(5):481–500.
[29] Fazelpour F, Tarashkar N, Rosen MA. Short-term wind speed forecasting using artificial neural networks for Tehran, Iran. Int J Energy Environ Eng 2016;7(4):377–90.
[30] Flato G, Marotzke J, Abiodun B, Braconnot P, Chou SC, Collins W, et al. Evaluation of climate models Climate change 2013: the physical science basis. Contribution of working group I to the fifth assessment report of the intergovernmental panel on climate change Cambridge, United Kingdom and New York, NY, USA. Cambridge University Press; 2013.
[31] Florides GA, Christodoulides P. Global warming and carbon dioxide through sciences. Environ Int 2009;35(2):390–401.
[32] Galloway JM, Wigston A, Patterson RT, Swindles GT, Reinhardt E, Roe HM. Climate change and decadal to centennial-scale periodicities recorded in a late Holocene NE Pacific marine record: Examining the role of solar forcing. Palaeogeogr Palaeoclimatol Palaeoecol 2013;386:669–89.
[33] Geirsdóttir Á, Miller GH, Thordarson T, Ólafsdóttir KB. A 2000 year record of climate variations 747 reconstructed from Haukadalsvatn, West Iceland. J Paleolimnol 2009;41:95–115.
[34] Gergis J, Neukom R, Gallant AJE, Karoly DJ. Australasian temperature reconstructions spanning the last millennium. J Climate 2016;29(15):5365–92.
[35] Gervais F. Anthropogenic CO_2 warming challenged by 60-year cycle. Earth-Sci Rev 2016;155:129–35.
[36] Guangliang H, Chongyi E, Xiangjun L, Fangming Z. Reconstruction of integrated temperature series of the past 2000 years on the Tibetan plateau with 10-year intervals. Theor Appl Climatol 2013;113:259–69.
[37] Hansen J, Ruedy R, Sato M, Lo K. Global surface temperature change. Rev Geophys 2010;48:RG4004.
[38] Harde H. Advanced two-layer climate model for the assessment of global warming by CO_2. Open J Atmos Clim Change 2014;1(3):1–50.
[39] Hargreaves JC, Annan JD, Yoshimori M, Abe-Ouchi A. Can the Last Glacial Maximum constrain climate sensitivity? Geophys Res Lett 2012;39:L24702.
[40] Hunt BG. The medieval warm period, the little ice age and simulated climatic variability. Clim Dyn 2006;27:677–94.
[41] Kamae Y, Shiogama H, Watanabe M, Ishii M, Ueda H, Kimoto M. Recent slowdown of tropical upper tropospheric warming associated with Pacific climate variability. Geophys Res Lett 2015;42(8):2995–3003.
[42] Larsen H, Froelich R. Ipiutak and the Arctic whale hunting culture. Am Museum Natural Hist 1948;42:1–276.
[43] Lamb HH. The earlier medieval warm epoch and its sequel. Palaeogeogr Palaeoclimatol Palaeoecol 1965;1:13–37.
[44] Lamb HH. Climate, history and the modern world. New York: Routledge; 1982.
[45] Laubereau A, Iglev H. On the direct impact of the CO_2 concentration rise to the global warming. Europhys Lett 2013;104(2):29001.
[46] Lewis N, Curry JA. The implications for climate sensitivity of AR5 forcing and heat uptake estimates. Clim Dyn 2014;45:1009–23.
[47] Lewis N. Implications of recent multimodel attribution for climate sensitivity. Clim Dyn 2016;46:1387–96.
[48] Lewis N. An objective bayesian improved approach for applying optimal fingerprint techniques to estimate climate sensitivity. J Climate 2013;26:7414–29.
[49] Li Q, Liu Y, Song H, Cai Q, Yang Y. Long-term variation of temperature over North China and its links with large-scale atmospheric circulation. Quatern Int 2013;283:11–20.
[50] Lightfoot HD, Mamer OA. Calculation of atmospheric radiative forcing (Warming Effect) of carbon dioxide at any concentration. Energy Environ 2014;25(8):1439–54.
[51] Lim H-G, Yeh S-W, Kim J-W, Park R, Song C-K. Contributions of solar and greenhouse gases forcing during the present warm period. Meteorol Atmos Phys 2014;126:71–9.
[52] Lindzen RS, Choi Y-S. On the observational determination of climate sensitivity and its implications. Asia-Pacific J Atmos Sci 2011;47(4):377–90.
[53] Ljungqvist FC. A new reconstruction of temperature variability in the extra-tropical Northern Hemisphere during the last two millennia. Geogr Ann A 2010;92:339–51.
[54] Ljungqvist FC, Krusic PJ, Brattstrom G, Sundqvist HS. Northern Hemisphere temperature patterns in the last 12 centuries. Clim Past 2012;8:227–49.
[55] Loehle C. A minimal model for estimating climate sensitivity. Ecol Model 2014;276:80–4.
[56] Luckman BH, Wilson RJS. Summer temperatures in the Canadian Rockies during the last millennium: a revised record. Clim Dyn 2005;24:131–44.
[57] Ma X, Jin Y, Dong Q. A generalized dynamic fuzzy neural network based on singular spectrum analysis optimized by brain storm optimization for short--term wind speed forecasting. Appl Soft Comput 2017;54:296–312.
[58] Mann ME, Bradley RS, Hughes MK. Northern hemisphere temperatures during the past millennium: inferences, uncertainties, and limitations. Geophys Res Lett 1999;26(6):759–62.
[59] Mann ME, Zhang Z, Hughes MK, Bradley MK, Miller SK, Rutherford S, et al. Proxy-based reconstructions of hemispheric and global surface temperature variations over the past two millennia. PNAS 2008;105(36):13252–7.
[60] Marohasy J, Abbot J. In: Easterbrook D, editor. Southeast australian maximum temperature trends, 1887–2013: an evidence-based reappraisal. Evidence-Based Climate Science; 2016. p. 83–99.
[61] Masters T. Observational estimates of climate sensitivity from changes in the rate of ocean heat uptake and comparison to CMIP5 models. Clim Dyn 2013;42(7-8):2173–81.
[62] Mathiassen T. The sermermiut excavations. Meddel 1958;161(3):1–52.
[63] Mathiassen T. Inugsuk, a medieval Eskimo settlement in Upernivik district, West Greenland. Meddel 1930;77(4):145–340.
[64] McShane BB, Wyner AJ. A statistical analysis of multiple temperature proxies: are reconstructions of surface temperatures over the last 1000 years reliable? Ann Appl Stat 2011;5(1):5–44.
[65] Mende W, Stellmacher R. Solar variability and the search for corresponding climate signals. Space Sci Rev 2000;94:295–306.
[66] Moberg A, Sonechkin DM, Holmgren K, Datsenko NM, Karlen W, Lauritzen SE. Highly variable Northern Hemisphere temperatures reconstructed from low and high resolution proxy data. Nature 2005;433:613–17.
[67] Moberg A. Comparisons of simulated and observed Northern Hemisphere temperature variations during the past millennium - selected lessons learned and problems encountered. Tellus B 2013;65:19921.
[68] Moffa-Sánchez P, Born A, Hall IR, Thornalley DJR, Barker S. Solar forcing of North Atlantic surface temperature and salinity over the past millennium. Nat Geosci 2014;7:275–8.
[69] Morellon M, Valero-Garces B, Gonzalez-Samperiz P, Vegas-Vilarrubia T, Rubio E, Rieradevall M. Climate changes and human activities recorded in the sediments of Lake Estanya (NE Spain) during the medieval warm period and little ice age. J Paleolimnol 2011;46:423–52.
[70] Mullins HT, Patterson WP, Teece MA, Burnett AW. Holocene climate and environmental change in central New York (USA). J Paleolimnol 2011;45:243–56.
[71] Myhre G, Shindell D, Bréon F-M, Collins W, Fuglestvedt J, Huang J, et al. Anthropogenic and natural radiative forcing Climate change 2013: The physical science basis. Contribution of working group I to the fifth assessment report of the intergovernmental panel on climate change Cambridge University Press Cambridge, United Kingdom and New York, NY, USA; 2013.
[72] Nayak DR, Mahapatra A, Mishra P. A survey on rainfall prediction using artificial neural network. Int J Comput Appl 2013;72(16):32–40.
[73] Neukom R, Luterbacher J, Villalba R, Kuttel M, Frank D, Jones PD, et al. Multiproxy summer and winter surface air temperature field reconstructions for southern South America covering the past centuries. Clim Dyn 2011;37(1-2):35–51.
[74] Nordemann DJR, Rigozo NR, de Faria HH. Solar activity and El-Nino signals observed in Brazil and Chile tree ring records. Adv Space Res 2005;35:891–6.
[75] Ogurtsov M, Lindholm M, Jalkanen R, Veretenenko SV. New evidence of solar variation in temperature proxies from Northern Fennoscandia. Adv Space Res 2013;52:1647–54.
[76] Pasini A, Lorè M, Ameli F. Neural network modelling for the analysis of forcings/temperatures relationships at different scales in the climate system. Ecol Model 2006;191:58–67.
[77] Priem HNA. CO_2 and climate: A geologist's view. Space Sci Rev 1997;81:173–98.
[78] Raspopov OM, Dergachev VA, Esperc J, Kozyreva OV, Frank D, Ogurtsov M, et al. The influence of the de Vries (~200-year) solar cycle on climate variations: Results from the Central Asian Mountains and their global link. Palaeogeogr Palaeoclimatol Palaeoecol 2008;259:6–16.
[79] Rigozoa NR, Nordemann DJR, da Silva EH, de Souza Echer MP, Echer E. Solar and climate signal records in tree ring width from Chile (AD 1587–1994). Planet Space Sci 2007;55:158–64.
[80] Sahin M. Modelling of air temperature using remote sensing and artificial neural network in Turkey. Adv Space Res 2012;50(7):973–85.
[81] Scafetta N. Problems in Modeling and forecasting climate change: CMIP5 general circulation models versus a semi-empirical model based on natural oscillations. Int J Heat Tech 2016;34(2):S435–42.
[82] Scafetta N. Discussion on climate oscillations: CMIP5 general circulation models versus a semi-empirical harmonic model based on astronomical cycles. Earth-Sci Rev 2013;126:321–57.
[83] Schmittner A, Urban NM, Shakun JD, Mahowald NM, Clark PU, Bartlein PJ, et al. Climate sensitivity estimated from temperature reconstructions of the last glacial maximum. Science 2011;334:1385–8.
[84] Skeie RB, Berntsen T, Aldrin M, Holdren M, Myhre G. A lower and more constrained estimate of climate sensitivity using updated observations and detailed radiative forcing time series. Earth Syst Dyn 2014;5:139–75.
[85] Specht DF. A general regression neural network. IEEE Trans Neural Netw 1991;2(6):568–76.
[86] Specht E, Redemann T, Lorenz N. Simplified mathematical model for calculating global warming through anthropogenic CO_2. Int J Therm Sci 2016;102:1–8.
[87] Stocker TF, Qin D, Plattner GK, Tignor M, Allen SK, Boschung J, et al., Climate change 2013: The physical science basis. Contribution of working group I to the fifth assessment report of the intergovernmental panel on climate change Cambridge University Press, Cambridge, United Kingdom and New York, NY, USA.
[88] Swingedouw D, Terray L, Cassou C, Voldoire A, Salas-Melia D. Natural forcing of climate during the last millennium: fingerprint of solar variability. Low frequency solar forcing and NAO. Clim Dyn 2011;36:1349–64.

[89] Tan M, Liu T. Cyclic rapid warming on centennial-scale revealed by a 2650-year stalagmite record of warm season temperature. Geophys Res Lett 2003;30(12):1617.
[90] Taricco C, Mancuso S, Ljungqvist FC, Alessio S, Ghil M. Multispectral analysis of Northern Hemisphere temperature records over the last five millennia. Clim Dyn 2015;45:83–104.
[91] Tei S, Yonenobu H, Shinya S, Motonari O, Katsuya G, Takeshi N, et al. Reconstructed July temperatures since AD 1800, based on a tree-ring chronology network in the Northwest Pacific region, and implied large-scale atmospheric–oceanic interaction. Clim Dyn 2010;35:953–63.
[92] Trachsel M, Grosjean M, Larocque-Tobler I, Schwikowski M, Blass A, et al. Quantitative summer temperature reconstruction derived from a combined biogenic Si and chironomid record from varved sediments of Lake Silvaplana (south-eastern Swiss Alps) back to AD 1177. Quaternary Sci Rev 2010;29:2719–30.
[93] Trouet V, Taylor AH. Multi-century variability in the Pacific North American circulation pattern reconstructed from tree rings. Clim Dyn 2010;35:953–63.
[94] van Geel B, Ziegler PA. IPCC Underestimates the Sun's role in climate change. Energy Environ 2013;24(3,4):431–53.
[95] van Hateren JH. A fractal climate response function can simulate global average temperature trends of the modern era and the past millennium. Clim Dynam 2013;40(11-12):2651–70.
[96] Vibe C. Arctic animals in relation to climatic fluctuations. Meddel 1967;170(5):1–227.
[97] Wilson R, Wiles G, D'Arrigo R, Zweck C. Cycles and shifts: 1300 years of multi-decadal temperature variability in the Gulf of Alaska. Clim Dyn 2007;28:425–40.
[98] Wilson DJ, Gea-Banacloche J. Simple model to estimate the contribution of atmospheric CO_2 to the Earth's greenhouse effect. Am J Phys 2012;80(4):306–15.
[99] Wu CL, Chau KW. Prediction of rainfall time series using modular soft computing methods. Eng Appl Artif Intel 2013;26:997–1007.
[100] Yamin W, Qi F, Xingcheng K. Tree-ring based reconstruction of temperature variability (1445–2011) for the upper reaches of the Heihe River Basin Northwest China. J Arid Land 2016;8(1):60–76.
[101] Yi L, Chen S, Ortiz JD, Chen G, Peng J, Liu F, et al. 1500-year cycle dominated Holocene dynamics of the Yellow River delta, China. Holocene 2016;26(2):222–34.
[102] Zhang Y, Shao XM, Yin Z-Y, Wang Y. Millennial minimum temperature variations in the Qilian Mountains, China: evidence from tree rings. Clim Past 2014;10:1763–78.
[103] Zhang J, Li L, Zhou T, Xin XG. Variation of surface temperature during the last millennium in a simulation with the FGOALS-gl climate system model. Adv Atmos Sci 2013;30(3):699–712.
[104] Zhou J, Tung K-K. Deducing multi-decadal anthropogenic global warming trends using multiple regression analysis. J Atmos Sci 2012;70(1):3–8.